European Radiology (2021) 31:8326–8334
https://doi.org/10.1007/s00330-021-07940-8

COMPUTED TOMOGRAPHY

Differentiating focal interstitial fibrosis from adenocarcinoma in persistent pulmonary subsolid nodules (> 5 mm and < 20 mm): the role of coronal thin-section CT images

Kai-Hsiung Ko[1] · Tsai-Wang Huang[2] · Wei-Chou Chang[1] · Hsu-Kai Huang[2] · Wen-Chiuan Tsai[3] · Hsian-He Hsu[1]

Received: 20 September 2020 / Revised: 25 February 2021 / Accepted: 25 March 2021 / Published online: 20 April 2021

Abstract

Objectives To investigate thin-section computed tomography (CT) features of pulmonary subsolid nodules (SSNs) with sizes between 5 and 20 mm to determine predictive factors for differentiating focal interstitial fibrosis (FIF) from adenocarcinoma.

Methods From January 2017 to December 2018, 169 patients who had persistent SSNs 5–20 mm in size and underwent preoperative nodule localization were enrolled. Patient characteristics and thin-section CT features of the SSNs were reviewed and compared between the FIF and adenocarcinoma groups. Univariable and multivariable analyses were used to identify predictive factors of malignancy. Receiver operating characteristic (ROC) curve analysis was used to quantify the performance of these factors.

Results Among the 169 enrolled SSNs, 103 nodules (60.9%) presented as pure ground-glass opacities (GGOs), and 40 (23.7%) were FIFs. Between the FIF and adenocarcinoma groups, there were significant differences ($p < 0.05$) in nodule border, shape, thickness, and coronal/axial (C/A) ratio. Multivariable analysis demonstrated that a well-defined border, a nodule thickness >4.2, and a C/A ratio >0.62 were significant independent predictors of malignancy. The performance of a model that incorporated these three predictors in discriminating FIF from adenocarcinoma achieved a high area under the ROC curve (AUC, 0.979) and specificity (97.5%).

Conclusions For evaluating persistent SSNs 5–20 mm in size, the combination of a well-defined border, a nodule thickness > 4.2, and a C/A ratio > 0.62 is strongly correlated with malignancy. High accuracy and specificity can be achieved by using this predictive model.

Key Points

- *Thin-section coronal images play an important role in differentiating FIF from adenocarcinoma.*
- *The combination of a well-defined border, nodule thickness>4.2 mm, and C/A ratio >0.62 is associated with malignancy.*
- *This predictive model may be helpful for managing persistent SSNs between 5 and 20 mm in size.*

Keywords Subsolid nodule · Focal interstitial fibrosis · Adenocarcinoma · Thin-section CT

Abbreviations

AAH	Atypical adenomatous hyperplasia
AIS	Adenocarcinoma in situ
AUC	Area under the ROC curve
CT	Computed tomography
FIF	Focal interstitial fibrosis
GGN	Ground-glass nodule
GGO	Ground-glass opacity
HU	Hounsfield units
MIA	Minimally invasive adenocarcinoma
PBD	Patent blue dye
ROC	Receiver operating characteristic
SSN	Subsolid nodule
VATS	Video-assisted thoracoscopic surgery

Tsai-Wang Huang and Hsian-He Hsu contributed equally to this work.

✉ Hsian-He Hsu
hsianhe@yahoo.com.tw

[1] Department of Radiology, Tri-Service General Hospital and National Defense Medical Center, 325, Section 2, Cheng-Gong Road, Nei-Hu, Taipei 114, Taiwan

[2] Department of Surgery, Division of Thoracic Surgery, Tri-Service General Hospital and National Defense Medical Center, Taipei, Taiwan

[3] Department of Pathology, Tri-Service General Hospital and National Defense Medical Center, Taipei, Taiwan

Introduction

The prevalence of subsolid nodules (SSNs) has gradually increased because of the widespread use of computed tomography (CT) for lung cancer screening and the improvement in computer technology. It is well known that persistent SSNs, including those with pure ground-glass opacity (GGO) and part-solid components, have a higher likelihood of malignancy than solid nodules [1]. Therefore, invasive procedures such as CT-guided core biopsy or video-assisted thoracoscopic surgery (VATS) are frequently required for tissue diagnosis. However, the diagnostic yield of CT-guided biopsy is low for small, deeply located or predominantly ground-glass nodules [2, 3]. With the advancements in preoperative nodule localization, VATS has become the mainstream method for diagnosing and treating SSNs [4, 5].

Pathologically, persistent SSNs usually represent malignant or precancerous lesions such as atypical adenomatous hyperplasia (AAH), adenocarcinoma in situ (AIS), minimally invasive adenocarcinoma (MIA), and invasive adenocarcinoma. The invasiveness of the nodule strongly correlates with the solid-to-tumor ratio on CT images [6, 7]. With regard to benign lesions, focal interstitial fibrosis (FIF) is the most common diagnosis and often shares similar radiological appearances with malignant SSNs according to previous reports and our experience [4, 5, 8]. In daily practice, it is sometimes difficult to differentiate FIF from a malignancy preoperatively. From a clinical perspective, a simple approach providing reliable criteria for dealing with this dilemma could help minimize unnecessary invasive diagnostic procedures. Although several studies have performed radiological-pathological analyses for benign and malignant SSNs with thin-section CT images and computer-aided techniques, variable results have been produced [9–12]. Furthermore, to the best of our knowledge, only a few studies with small sample sizes have been published assessing the CT features of FIF [13–15]. Hence, the purpose of this study is to investigate thin-section CT manifestations of persistent SSNs to determine predictive factors for differentiating FIF from adenocarcinoma and AAH.

Materials and methods

This study was approved by the Institutional Review Board, and informed consent was waived because of the observational and retrospective nature of the study. The CT findings and pathological records of patients who underwent VATS at our institute for pulmonary nodules between January 2017 and December 2018 were reviewed. The inclusion criteria were as follows: (1) lesions presenting as pure ground-glass nodules (GGNs) or part-solid GGNs on initial CT images and persisting over a follow-up of 3 months or longer; (2) nodule size > 5 mm and < 20 mm; (3) pathologic report describing terms including FIF, AAH, AIS, MIA, or invasive adenocarcinoma; (4) preoperative nodule localization performed; and (5) pre- and postoperative CT images available in the picture archiving and communication system (PACS) (EBM Technologies Incorporated). The surgical intervention was performed according to the following conditions: (1) growing nodules; (2) increasing solid component of nodules; (3) indeterminate nodules that were recommended by multidisciplinary discussion; or (4) patients who were anxious about malignant potential requested the surgery.

A total of 353 patients underwent VATS for indeterminate pulmonary nodules. Among them, 184 patients were excluded for the following reasons: (1) the presence of a solid nodule (n=89); (2) nodule size <5 mm or > 20 mm (n=38); (3) no preoperative nodule localization performed (n=41); and (4) unavailable preoperative CT images (n=16). Finally, 169 patients who met all inclusion criteria were enrolled in this study. The basic profiles of each patient, including age, sex, smoking status, and type of surgical intervention (i.e., wedge resection, segmentectomy, or lobectomy), were recorded.

CT technique

All CT examinations were performed by using a 256-detector row CT scanner (Brilliance iCT; Philips) and a 64-detector row scanner (Brilliance; Philips Medical Systems). Patients were kept in the supine position with full inspiration during scanning. The CT parameters were as follows: tube voltage, 120 kVp; tube current, 60–90 mAs; detector collimation, 0.625–1.25 mm; beam pitch, 1.05–1.25; rotation time, 0.6–0.8 s. All image data were reconstructed using the kernel of a high-frequency reconstruction algorithm with slice thickness ≤ 1.5 mm. Preoperative nodular localization was performed with CT-guided patent blue dye (PBD) injection as described in detail in our previous study [5]. After the operation, follow-up CT images were routinely obtained to confirm complete resection of the nodule.

Analysis of thin-section CT image features

The CT findings were analyzed in the lung window setting (window level, −600 Hounsfield units (HU); window width, 1500 HU) using a PACS workstation. All thin-section CT images were independently reviewed by two chest radiologists (H.H.H. and K.K.H., with 30 and 15 years of experience, respectively) who were blinded to the clinical information and pathological diagnosis of the patient. The imaging features analyzed for each lesion included the following: (a) nodule size, (b) nodule location (parenchyma or subpleural), (c) matrix (pure GGO or part-solid), (d) border (well-defined or ill-defined), (e) margin (spiculated or non-spiculated), (f) shape (oval or round, irregular or polygonal), (g) presence of pleural

tags, (h) presence of emphysema, (i) nodule thickness, and (j) coronal/axial (C/A) ratio. Nodules located less than 1 cm from the pleura were recognized as having a subpleural location. GGO referred to a hazy opacity that preserved the background structures. Part-solid referred to a GGN combined with a solid component. An ill-defined border was defined as an indistinct interface between the nodule and adjacent parenchyma. A spiculated margin was defined as a thickening and distorted line radiating from the nodular surface. A pleural tag was defined as a linear strand that extended from the nodular surface to the pleura. Nodule size was measured as the maximal dimension on axial images. Nodule thickness was measured as the maximal dimension in the cephalocaudal direction on coronal images. The C/A ratio was defined as the ratio of the maximal thickness of the lesion to its maximal axial diameter (Fig. 1). Quantitative measurements were performed by each reviewer using an electronic calliper under 500% zoom magnification to determine the nodule size, thickness, and C/A ratio. The average value of both reviewers' measurements was recorded as the final result. If the interobserver difference was outside the limits of agreement, an additional measurement was conducted by consensus.

Statistical analyses

Descriptive data are expressed as the means ± standard deviations. Differences between the FIF and adenocarcinoma groups were assessed with the chi-squared and Fisher's exact tests for categorical variables and the independent samples *t* test for continuous variables. Interobserver agreement for morphologic analysis was assessed using the kappa statistic. The kappa value was recognized as poor (<0.20), fair (0.21–0.40), moderate (0.41–0.60), good (0.61–0.80), and excellent (0.81–1.00) [16]. Bland-Altman plots were generated to assess the interobserver variability of measuring nodule size and thickness [17]. Receiver operating characteristic (ROC) curves were generated for the nodule thickness and C/A ratio to determine the cut-off value that yielded optimal values of sensitivity and specificity. Multivariable logistic regression analysis using the enter method was performed to identify independent predictive factors of malignancy. The predictive performance of the established model in discriminating malignancy from FIF was evaluated by calculating the area under the ROC curve (AUC), as described by Hanley and McNeil [18]. *p* values of less than 0.05 were considered statistically significant. All statistical analyses were performed using SPSS software (version 20.0; SPSS) and MedCalc (MedCalc).

Results

Patient characteristics

The characteristics of the 169 enrolled patients with 169 subsolid nodules are shown in Table 1. The mean diameter of the nodules was 9.9 mm (range, 5.2–19 mm). Among them, 103 nodules (60.9%) presented as pure GGOs, and 66 nodules (39.1%) presented with a part-solid appearance. The majority of the patients underwent sublobar resections, including wedge resection (n = 104; 61.5%) and segmentectomy (n = 48; 28.4%). The majority of the histological malignancy subtypes were invasive adenocarcinoma (n =85; 50.3%), followed by MIA (n = 23; 13.6%), AIS (n = 16; 9.5%), and AAH (n = 5; 3.0%). The remaining nodules were FIFs (n = 40; 23.7%).

Thin-section CT features of FIF and adenocarcinoma groups

The kappa values of the two reviewers for CT morphologic evaluation showed good to excellent agreement and were as

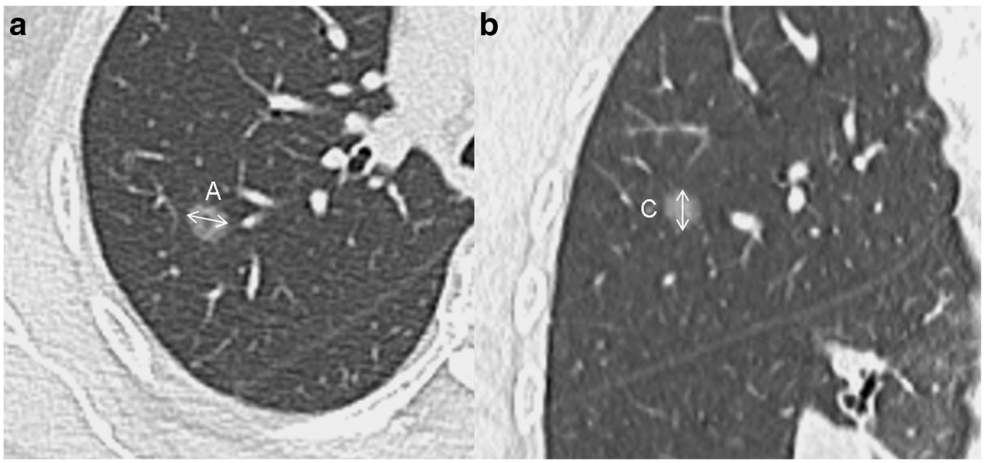

Fig. 1 Representative images of calculating C/A ratio and measuring nodule thickness of the nodule. (a) The longest diameter of the nodule in the axial plane is recognized as A. (b) The nodule thickness refers to the maximal distance between the cranial and caudal margin of the nodule in the coronal plane, which is recognized as C

Table 1 Patient characteristics

Characteristics	No. of patients $n = 169$
Age, mean (range)	61.3 (33–84)
Sex	
Male	55
Female	114
Smoke status	
Never	120
Current or former	49
Nodule size (mm)	
Mean (range)	9.9 (5.2–19)
Nodule type	
Pure GGO	103
Part-solid	66
Operation	
Wedge resection	104
Segmentectomy	48
Lobectomy	17
Histology	
FIF	40
AAH	5
AIS	16
MIA	23
IA	85

GGO, ground-glass opacity; *FIF*, focal interstitial fibrosis; *AAH*, atypical adenomatous hyperplasia; *AIS*, adenocarcinoma in situ; *MIA*, minimally invasive adenocarcinoma; *IA*, invasive adenocarcinoma

follows: 0.675 (95% CI: 0.561, 0.790) for matrix, 0.788 (95% CI: 0.683, 0.894) for border, 0.848 (95% CI: 0.679, 0.959) for margin, 0.744 (95% CI: 0.658, 0.830) for shape, and 0.747 (95% CI: 0.640, 0.855) for pleural tag. Figure 2 demonstrates the Bland-Altman plots for measuring nodule size and thickness. The mean difference in size measurements was 0.43 mm with a lower limit of agreement of −0.82 mm and an upper limit of agreement of 1.68 mm. The mean difference in thickness measurements was 0.14 mm with a lower limit of agreement of −0.90 mm and an upper limit of agreement of 1.18 mm. The mean differences of both measurements were close to zero and the range of the 95% limits of agreement was acceptably narrow, indicating good interobserver agreement. When comparing the CT features of FIF with those of adenocarcinoma and AAH, ROC curve analysis demonstrated that the cut-off values for nodule thickness and the C/A ratio were 4.2 and 0.62, respectively. The calculated AUC of nodule thickness was 0.89 (sensitivity=77.5%; specificity=97.7%), indicating good discrimination, and that of the C/A ratio was 0.93 (sensitivity=90.0%; specificity=86.8%), indicating perfect discrimination. Among all CT features, there were significant differences in nodule border, shape, thickness, and C/A ratio between the two groups (Table 2). The adenocarcinoma groups predominantly presented with well-defined borders (80.6% vs. 42.5%, p= 0.012), round or oval and polygonal shapes (65.1% vs. 60.0% and 27.9% vs. 12.5%, p=0.001), a nodule thickness > 4.2 mm (96.1% vs. 25.0%, $p < 0.001$), and a C/A ratio > 0.62 (88.4% vs. 12.5%, $p < 0.001$) (Figs. 3 and 4). Other imaging features, including nodule size, matrix, and margin and the presence of emphysema and pleural tags, were not significantly different between groups.

Multivariable logistic regression analysis for discriminating adenocarcinoma and AAH from FIF

Age, sex, smoking status, nodule border, nodule shape, nodule thickness, and the C/A ratio were selected for multivariable logistic regression analysis. The results revealed that age, sex, smoking status, and nodule shape were not statistically significant, whereas a well-defined nodule border, a nodule thickness > 4.2 mm, and a high C/A ratio (>0.62) were significantly associated with adenocarcinoma and AAH (Table 3). ROC curve analysis was used to evaluate the predictive value of the logistic regression model generated with these three variables in discriminating adenocarcinoma and AAH from FIF, and the AUC increased to 0.979 (sensitivity=85.3%; specificity=97.5%, $p < 0.001$). This result suggested that with the combination of nodule border, nodule thickness, and C/A ratio, this predictive model demonstrated better discriminative power than individual features alone, such as nodule thickness or C/A ratio (Fig. 5). Furthermore, with regard to FIF, a higher specificity (97.5%) could also be attained with this model (Fig. 6).

Discussion

The increase in tissue diagnoses for persistent subsolid nodules has resulted in an increase in the incidence of FIF because it shares many radiological features of malignancy. Therefore, it is crucial to establish reliable criteria to differentiate FIF from malignancy to avoid unnecessary invasive diagnostic procedures. The present study revealed a simple predictive model for persistent SSNs between 5 and < 20 mm that could differentiate adenocarcinoma and AAH from FIF. The four main findings were as follows: (1) A nodule with a well-defined border was more frequently present with malignancy. (2) A nodule thickness ≤4.2 mm tended to be associated with FIF. (3) A nodule C/A ratio >0.62 was highly associated with malignancy. (4) The combination of these three predictors could perfectly discriminate FIF from malignancy. Although some studies with smaller sample sizes have attempted to

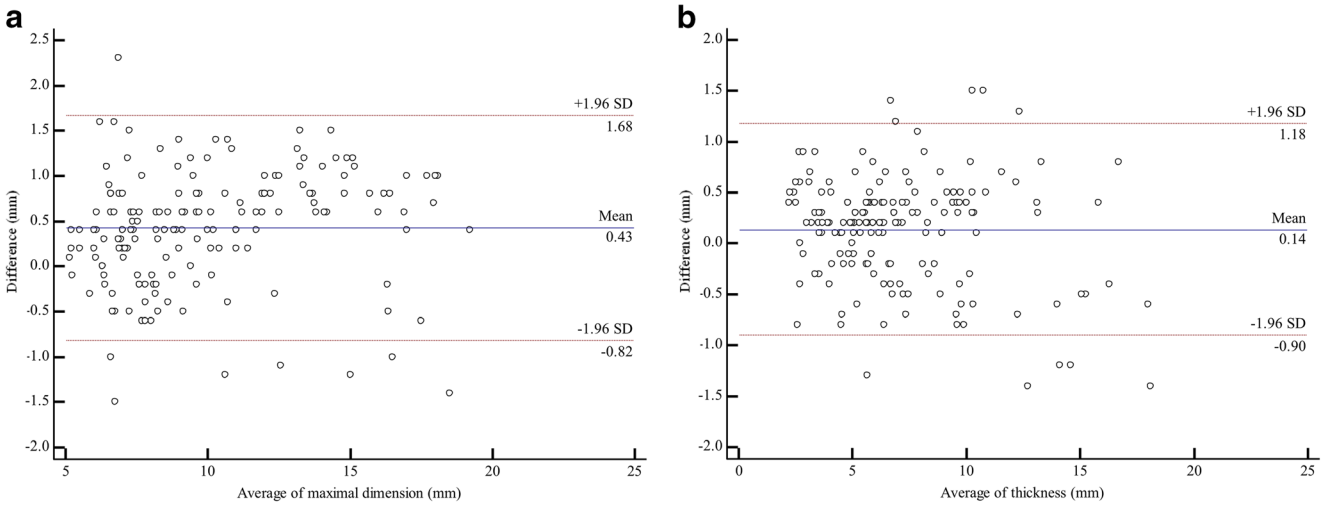

Fig. 2 Bland-Altman plots show the maximal nodule size (a) and thickness (b) measurements performed by two reviewers

differentiate FIFs from malignant SSNs based on imaging features, their results have varied. Takashima et al [13] and Si et al [14] reported that a concave margin and a polygonal shape were features of FIF. On the other hand, Park et al [15] more commonly noted a round or oval shape in their FIF nodules. The results of our study are consistent with the description of Park et al [15], but the nodule shape did not show statistical significance in multivariable analysis. There are several possible reasons for this discrepancy. First, the interobserver variability may exist between different studies. Second, the inclusion criteria of each study were different. Takashima et al [13] included not only SSNs but also solid nodules. Finally, several nodules in our study manifested ill-defined borders, which may have hampered the correct evaluation of nodule shape.

Table 2 Thin-section CT features of FIF and adenocarcinoma groups

Variables	FIF (n = 40)	Adenocarcinoma and AAH (n = 129)	p value
Nodule size (mm)	9.3±3.1	10.1±3.6	0.12
Emphysema			
Yes	5	7	0.158
No	35	122	
Location			
Parenchymal	18	69	0.371
Subpleural	22	60	
Matrix			
Pure GGO	24	79	0.964
Part-solid	16	50	
Border			
Ill-defined	23	25	0.012
Well-defined	17	104	
Margin			
Spiculated	2	10	0.734
Nonspiculated	38	119	
Shape			
Oval or round	24	84	0.001
Irregular	11	9	
Polygonal	5	36	
Pleural tag			
Yes	16	42	0.447
No	24	87	
Nodule thickness (mm)			
> 4.2	10	124	< 0.001
≤ 4.2	30	5	
Nodule C/A ratio			
> 0.62	5	114	< 0.001
≤ 0.62	35	15	

FIF, focal interstitial fibrosis; *AAH*, atypical adenomatous hyperplasia; *GGO*, ground-glass opacity; *C/A*, coronal/axial

The nodule border has been investigated in some studies, which collectively indicated that a well-defined SSN interface or margin was more suggestive of malignancy [11, 19]. In the present study, although approximately half of the FIF nodules showed a well-defined border, the frequency of well-fined borders for malignancies was significantly greater than that for FIF. Pathologically, cancer cells infiltrate the peripheral region of the tumor, causing abrupt thickening of the alveolar wall, which is hindered by interlobular septa and results in a well-defined border. Conversely, FIFs may undergo inflammatory reactions that gradually diminish in the periphery, which may be related to the formation of an ill-defined border [11]. Therefore, based on the results of the present and previous studies, the nodule border could be recognized as a useful discriminator for persistent SSNs.

To accurately measure and characterize pulmonary nodules, it has been recommended that thin-section images be obtained to minimize partial volume effects, which may cause the misinterpretation of solid nodules as SSNs [20]. Furthermore, reconstructing images with an additional coronal plane can help evaluate the craniocaudal extents of SSNs and facilitate the differentiation of focal fibrotic scars or plate-like atelectasis from true lesions [20]. Thus, although adenocarcinoma and FIF

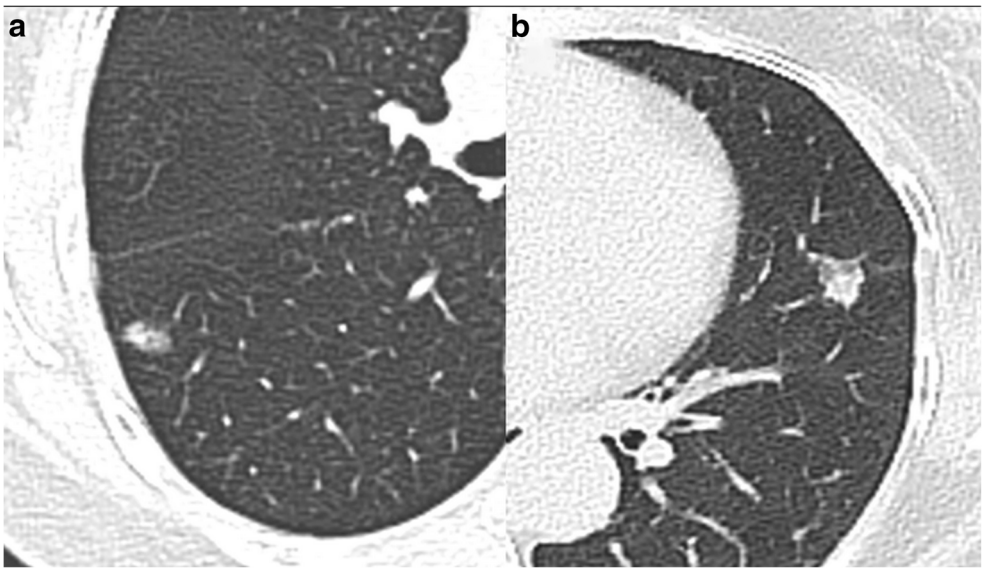

Fig. 3 Axial thin-section CT images show malignant persistent SSNs with oval or polygonal shapes. (a) The image of a 60-year-old woman shows a 9.3-mm part-solid GGN with a well-defined border and oval shape in the right lower lobe. (b) The image of a 65-year-old woman shows a 12-mm part-solid GGN with a polygonal shape and well-defined border in the left upper lobe. These two nodules were proven to be invasive adenocarcinomas via segmentectomy

may display similar imaging features as persistent SSNs, the growth patterns in the third dimension might be different, but measurement of the extent of both entities in the coronal plane has never been emphasized in the

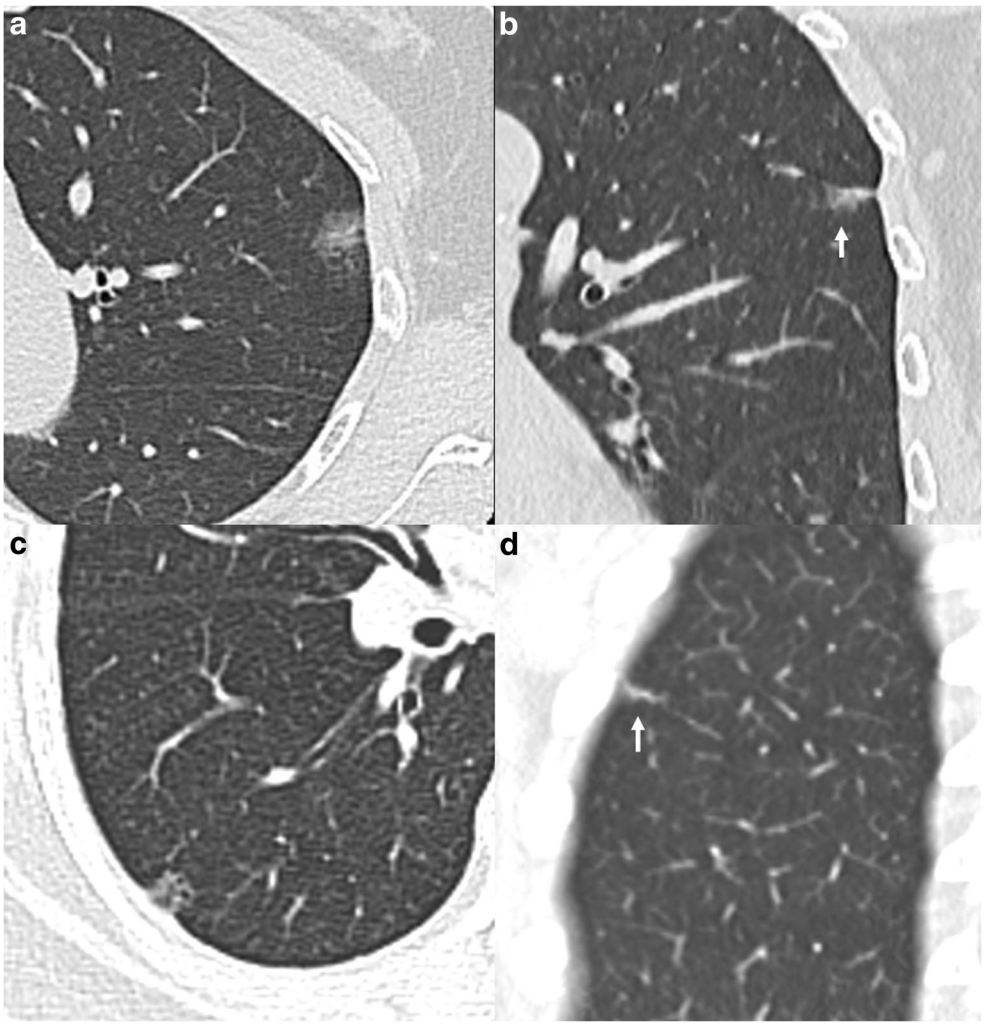

Fig. 4 The difference in the nodule thickness and C/A ratio between malignant and FIF SSNs. (a) The axial thin-section image of a 48-year-old woman with invasive adenocarcinoma shows a 10.7-mm pure ground-glass nodule with a well-defined border in the left upper lobe. (b) The coronal image shows a relatively flat configuration (arrow) with 6.8-mm thickness. The calculated C/A ratio is 0.64. (c) The axial thin-section image of a 70-year-old man with FIF shows a 8.2-mm pure ground-glass nodule with a well-defined border in the right lower lobe. (d) The coronal image shows a band-like appearance (arrow) with 3.2-mm thickness. The calculated C/A ratio is 0.39

Table 3 Multivariable analysis for predictive factors of adenocarcinoma and AAH

Variables	Adenocarcinoma and AAH (n = 129)	FIF (n = 40)	OR (95% CI)	p value
Age	60.9±10.1	62.66±9.9	1.00 (0.92–1.09)	0.932
Sex			0.17 (0.01–3.09)	0.234
Male	38	17		
Female	91	23		
Smoke status			1.20 (0.07–20.17)	0.900
Never	92	27		
Current or former	37	13		
Border			11.16 (1.99–62.59)	0.006
Ill-defined	25	23		
Well-defined	104	17		
Shape			1.22 (0.45–3.31)	0.695
Oval or round	84	24		
Irregular	9	11		
Polygonal	36	5		
Nodule thickness (mm)			82.86 (12.16–564.52)	< 0.001
> 4.2	124	10		
≤ 4.2	5	30		
Nodule C/A ratio			90.55 (11.9–689.11)	< 0.001
> 0.62	114	5		
≤ 0.62	15	35		

AAH, atypical adenomatous hyperplasia; *FIF*, focal interstitial fibrosis; *OR*, odds ratio; *CI*, confidence interval; *C/A*, coronal/axial

literature. In the present study, we presume that coronal plane images play an important role in differentiating FIF from adenocarcinoma. The results show that a nodule thickness >4.2 mm is an independent predictor of malignancy. Moreover, regarding the three-dimensional evaluation of the nodule, we also found that malignant SSNs had a higher C/A ratio than FIF, with the threshold for discrimination identified as 0.62. Both results indicate that nodules with flat or band-like appearances in coronal images have an increased likelihood of being FIFs. Otherwise, malignancies tend to have a spherical configuration and be thicker in coronal images. Takashima et al [13] mentioned a similar concept when applied to nodules less than 1 cm. Although their three-dimensional ratio threshold is close to ours (0.56 vs. 0.62) and was highly specific in identifying benignity, the sensitivity of their criterion is much lower than ours (63% vs. 85.3%). The possible reasons could be explained as follows: first, their sample size was relatively small, and most of their nodules were solid; second, their study included nodules smaller than 5 mm; finally, regarding benignity, they investigated not only FIF but also other entities, such as organizing pneumonia, granuloma, or intrapulmonary lymph nodes. Regardless of the discrepancies between the studies, the evidence demonstrates that measuring nodule thickness and the C/A ratio with coronal images facilitates the evaluation of persistent SSNs.

Compared with previous studies, the predictive model we established has several advantages: (a) All nodules were diagnosed via CT-guided preoperative localization, which had not been demonstrated in previous studies. The failure rate of nodular detection during surgery can reach approximately 60% without preoperative localization, especially when the nodule is less than 10 mm in size, possesses a predominantly ground-glass component, and is located far from the visceral pleura [21]. Therefore, it is important to perform preoperative localization to confirm the diagnosis of SSN. (b) The sample size of FIF nodules in our study is larger than that in previous studies. (c) The three predictors that significantly differentiated FIF from adenocarcinoma can achieve a reliable predictive value when taken together with a specificity of 97.5% and a high AUC of 0.979. (d) The measuring process of this model is simple and reproducible and does not require advanced technologies. Thus, we hope this predictive model will enable both clinicians and radiologists to manage persistent SSNs more confidently and efficiently and avoid unnecessary invasive procedures.

This study has some limitations. First, selection bias may be present due to the retrospective nature of the

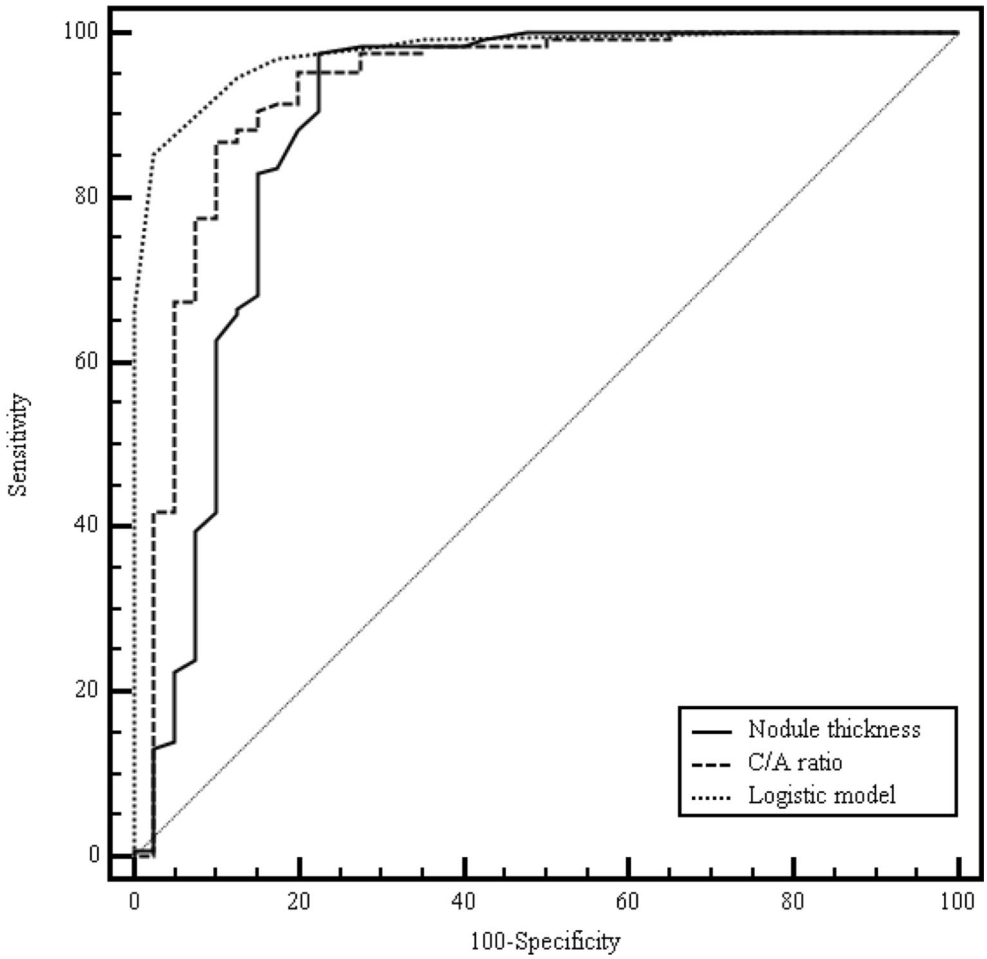

Fig. 5 The AUC of the logistic model including the nodule border, nodule thickness, and C/A ratio is higher (AUC=0.98) than the AUC of the nodule thickness (AUC=0.89) or C/A ratio (AUC=0.93) alone

study. Second, the sample size of this study is small, and a large-scale, prospective study is warranted to validate the present results. Third, we only investigated FIFs, and whether the established criteria can be applied to other benign SSNs should be investigated with further research. Finally, nodules less than 5 mm in size were not included in this study. However, according to updated Fleischner Society Guidelines for managing small

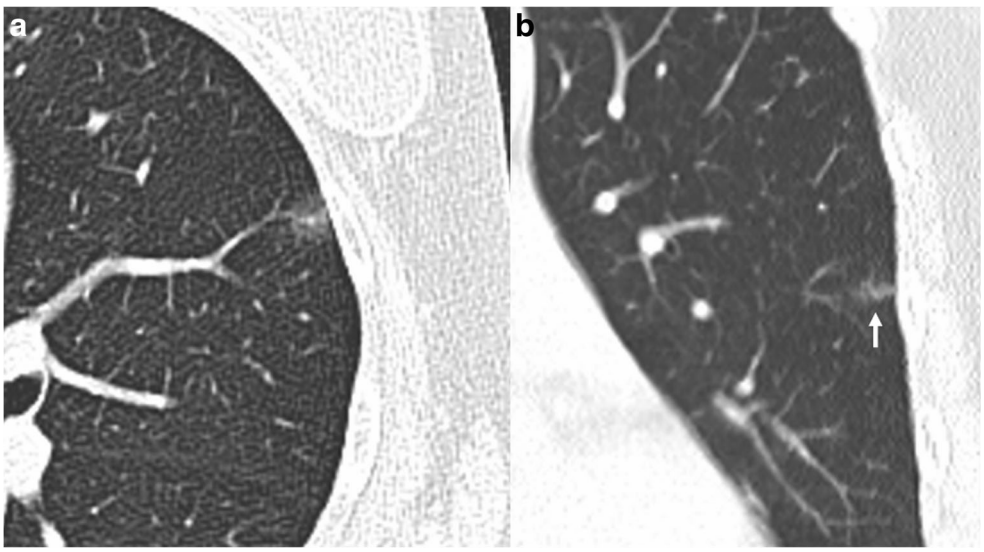

Fig. 6 The representative images of FIF in a 50-year-old woman. (a) The axial thin-section image shows a 8.3-mm ground-glass nodule with an ill-defined border in the left upper lobe. (b) The coronal image shows that the nodule thickness (arrow) is 3.7 mm and the calculated C/A ratio is 0.45

solitary SSNs, no routine follow-up is necessary because the data from the Nelson trial demonstrated that the malignant risk of nodules less than 5 mm in size is less than 1% [20, 22].

In conclusion, the results of our study highlight the predictive value of coronal thin-section images for persistent SSNs in differentiating FIF from adenocarcinoma and reveal that a well-defined border, nodule thickness >4.2 mm, and C/A ratio >0.62 are strongly associated with malignancy. A predictive model combining these three predictors can achieve perfect discrimination between the two entities with high accuracy.

Funding None.

Declarations

Guarantor The scientific guarantor of this publication is Hsian-He Hsu.

Conflict of interest The authors of this manuscript declare no relationships with any companies, whose products or services may be related to the subject matter of the article.

Statistics and biometry One of the authors has significant statistical expertise.

No complex statistical methods were necessary for this paper.

Informed consent Written informed consent was waived by the Institutional Review Board.

Ethical approval Institutional Review Board approval was obtained.

Methodology
- retrospective
- diagnostic study
- performed at one institution

References

1. McWilliams A, Tammemagi MC, Mayo JR et al (2013) Probability of cancer in pulmonary nodules detected on first screening CT. N Engl J Med 369:910–919
2. Shimizu K, Ikeda N, Tsuboi M, Hirano T, Kato H (2006) Percutaneous CT-guided fine needle aspiration for lung cancer smaller than 2cm and revealed by ground-glass opacity at CT. Lung Cancer 51:173–179
3. Inoue D, Gobara H, Hiraki T et al (2012) CT fluoroscopy-guided cutting needle biopsy of focal pure ground-glass opacity lung lesions: Diagnostic yield in 83 lesions. Eur J Radiol 81:354–359
4. McDermott S, Fintelmann FJ, Bierhals AJ et al (2019) Image-guided preoperative localization of pulmonary nodules for video-assisted and robotically assisted surgery. Radiographics 39:1264–1279
5. Ko KH, Huang TW, Lee SC, Chang WC, Gao HW, Hsu HH (2019) A simple and efficient method to perform preoperative pulmonary nodule localization: CT-guided patent blue dye injection. Clin Imaging 58:74–79
6. Suzuki K, Koike T, Asakawa T et al (2011) A prospective radiological study of thin-section computed tomography to predict pathological noninvasiveness in peripheral clinical IA lung cancer (Japan clinical oncology group 0201). J Thorac Oncol 6:751–756
7. Lee SM, Park CM, Goo JM, Lee HJ, Wi JY, Kang CH (2013) Invasive pulmonary adenocarcinomas versus preinvasive lesions appearing as ground-glass nodules: Differentiation by using CT features. Radiology 268:265–273
8. Goo JM, Park CM, Lee HJ (2011) Ground-glass nodules on chest CT as imaging biomarkers in the management of lung adenocarcinoma. Am J Roentgenol 196:533–543
9. Takashima S, Sone S, Li F, Maruyama Y, Hasegawa M, Kadoya M (2003) Indeterminate solitary pulmonary nodules revealed at population-based CT screening of the lung: Using first follow-up diagnostic CT to differentiate benign and malignant lesions. Am J Roentgenol 180:1255–1263
10. Kim HY, Shim YM, Lee KS, Han J, Yi CA, Kim YK (2007) Persistent pulmonary nodular ground-glass opacity at thin-section CT: Histopathologic comparisons. Radiology 245:267–275
11. Fan L, Liu SY, Li QC, Yu H, Xiao XS (2012) Multidetector CT features of pulmonary focal ground-glass opacity: Differences between benign and malignant. Br J Radiol 85:897–904
12. Kim KG, Goo JM, Kim JH et al (2005) Computer-aided diagnosis of localized ground-glass opacity in the lung at CT: Initial experience. Radiology 237:657–661
13. Takashima S, Sone S, Li F et al (2003) Small solitary pulmonary nodules (< or =1 cm) detected at population-based CT screening for lung cancer: Reliable high-resolution CT features of benign lesions. Am J Roentgenol 180:955–964
14. Si MJ, Tao XF, Du GY et al (2016) Thin-section computed tomography–histopathologic comparisons of pulmonary focal interstitial fibrosis, atypical adenomatous hyperplasia, adenocarcinoma in situ, and minimally invasive adenocarcinoma with pure ground-glass opacity. Eur J Radiol 85:1708–1715
15. Park CM, Goo JM, Lee HJ et al (2007) Focal interstitial fibrosis manifesting as nodular ground-glass opacity: Thin-section CT findings. Eur Radiol 17:2325–2331
16. Landis JR, Koch GG (1977) The measurement of observer agreement for categorical data. Biometrics 33:159–174
17. Bland JM, Altman DG (1986) Statistical methods for assessing agreement between two methods of clinical measurement. Lancet 1:307–310
18. Hanley JA, McNeil BJ (1982) The meaning and use of the area under a receiver operating characteristic (ROC) curve. Radiology 143:29–36
19. Nambu A, Araki T, Taguchi Y et al (2005) Focal area of ground-glass opacity and ground-glass opacity predominance on thin-section CT: Discrimination between neoplastic and non-neoplastic lesions. Clin Radiol 60:1006–1017
20. MacMahon H, Naidich DP, Goo JM et al (2017) Guidelines for management of incidental pulmonary nodules detected on CT images: From the Fleischner Society 2017. Radiology 284:228–243
21. Suzuki K, Nagai K, Yoshida J et al (1999) Video-assisted thoracoscopic surgery for small indeterminate pulmonary nodules: Indications for preoperative marking. Chest 115:563–568
22. Horeweg N, van Rosmalen J, Heuvelmans MA et al (2017) Lung cancer probability in patients with CT-detected pulmonary nodules: A prespecified analysis of data from the NELSON trial of low-dose CT screening. Lancet Oncol 15:1332–1341